Research Article Vol. 31, No. 9 / 24 Apr 2023 / Optics Express 13528
Optics EXPRESS

Identification of orbital angular momentum using atom-based spatial self-phase modulation

WEI GAO,[1,2] SANDAN WANG,[1,2] JINPENG YUAN,[1,2,3] LIANTUAN XIAO,[1,2] SUOTANG JIA,[1,2] AND LIRONG WANG[1,2,*]

[1]*State Key Laboratory of Quantum Optics and Quantum Optics Devices, Institute of Laser Spectroscopy, Shanxi University, 92 Wucheng Road, Taiyuan 030006, China*
[2]*Collaborative Innovation Center of Extreme Optics, Shanxi University, 92 Wucheng Road, Taiyuan 030006, China*
[3]*yjp@sxu.edu.cn*
[*]*wlr@sxu.edu.cn*

Abstract: Optical vortex orbital angular momentum modes, namely the twists number of the light does in one wavelength, play a critical role in quantum-information coding, super-resolution imaging, and high-precision optical measurement. Here, we present the identification of the orbital angular momentum modes based on spatial self-phase modulation in rubidium atomic vapor. The refractive index of atomic medium is spatially modulated by the focused vortex laser beam, and the resulted nonlinear phase shift of beam directly related to the orbital angular momentum modes. The output diffraction pattern carries clearly distinguishable tails, whose number and rotation direction correspond to the magnitude and sign of the input beam orbital angular momentum, respectively. Furthermore, the visualization degree of orbital angular momentums identification is adjusted on-demand in the terms of incident power and frequency detuning. These results show that the spatial self-phase modulation of atomic vapor can provide a feasible and effective way to rapidly readout the orbital angular momentum modes of vortex beam.

1. Introduction

Photons carries orbital angular momentum (OAM) and spin angular momentum (SAM) with quantum state information from a microscopic perspective [1–3]. The OAM is generated from twisted phase fronts arising due to spatially varying phase distribution across the beam [4]. Vortex beams with OAM exhibit helical phase structures $exp(i\ell\varphi)$ and central singularities, where φ is the azimuthal angle, and ℓ is the topological charge representing the OAM mode. As an unlimited integer value, the ℓ provides an infinite quantity of the achievable OAM state, promising considerable application prospects in the fields of optical manipulation, quantum information processing, and free-space optical communications [5–10].

The identification of the OAM modes is always accompanied by optical interference and diffraction effects [11–14]. The interference effect-based methods measure the OAM modes through the special fringe generated by the interaction between the vortex beam and the reference beam with a complicated experimental setup. The optical diffraction-based methods identify the OAM modes via the diffraction pattern of the vortex beam with propagation direction deviation after passing through diffraction elements with lower diffractive efficiency and complex aperture structure. As an alternative, the beam spatial distribution evolution caused by spatial self-phase modulation effect in nonlinear media also provides another way for the identification of the OAM modes intuitively [15]. The spatial self-phase modulation is usually employed to produce phase shift by varying refractive index when the vortex beams interact with the media, which will lead to various nonlinear diffraction patterns carrying OAM modes information.

#482116 https://doi.org/10.1364/OE.482116
Journal © 2023 Received 28 Nov 2022; revised 24 Mar 2023; accepted 24 Mar 2023; published 11 Apr 2023

Optics EXPRESS

The spatial self-phase modulation of exotic nonlinear two-dimensional materials, such as graphene, $TaSe_2$ nanosheets, $NbSe_2$ nanosheets, and GeSe nanoflakes, have been applied for performing all-optical devices [16–22]. And the spatial self-phase modulation in layered WS_2 nanosheets is employed for vortex beam OAM modes recognition recently [23]. Compared with two-dimensional materials, atomic vapor exhibits the novel characteristics as a nonlinear medium. Firstly, the easily saturated characteristic of atomic medium makes it favorable to observe nonlinear effects at low power. Secondly, the flexible tunability of atomic medium is enabled by the rich hyperfine energy level structure. Finally, the wonderful nonlinear atomic system with typical nonlinear effects of electromagnetically induced transparency, self-focusing, and self-trapping is promoting the realization and application of atom-based optical communications and all-optical devices [24–33]. These advantages make the spatial self-phase modulation effect in atomic medium provide a convenient and highly effective approach for simultaneously detecting OAM modes with arbitrary magnitude and sign. To our best knowledge, the readout of OAM modes based on spatial self-phase modulation in atomic medium has not been investigated experimentally yet.

In this work, we present the identification of OAM modes using Rb vapor-based spatial self-phase modulation. When the vortex beam interacts with the atomic medium, the nonlinear phase shift of beam directly related to the OAM modes is induced by taking advantage of the spatial self-phase modulation. As a result, the identification of OAM modes is realized by the diffraction patterns with clearly distinguishable tails. The magnitude and sign of vortex beam OAM modes with $|\ell|$ from 1 to 5 are determined by the number and direction of the obtained tails, respectively. Furthermore, the visualization degree of OAM modes identification is investigated via the adjusted profile area of the diffraction patterns in real-time. This OAM modes identification method based on spatial self-phase modulation in atomic vapor is capable of measuring high-order modes, indicating its application in large-capacity optical communication.

2. Experimental setup

The experimental setup for OAM modes identification based on spatial self-phase modulation in Rb vapor is demonstrated in Fig. 1(a). The laser source is provided by an external cavity diode laser (DL pro, Toptica) with a 780 nm Gaussian beam, which is utilized to excite the Rb atoms from $5S_{1/2}$ ground state to $5P_{3/2}$ excited state. The laser beam is split into two components with the combination of half-wave plate (HWP) and polarization beam splitter (PBS). One beam is employed to monitor the laser frequency using a wavelength meter (WS-7, HighFinesse). The other beam is firstly converted into circularly polarized light through a quarter-wave plate (QWP), then the vortex beams with different OAM modes are generated through the well-known optical converting q-plates with polarization-dependent optical properties [34]. The generated vortex beam with about 0.7 mm waist is focused through a lens with focal length of 150 mm, which makes the beam waist ω_0 of 53 μm and the Rayleigh length z_R of 12 mm. The Rb vapor cube cell with $20 \times 20 \times 20$ mm^3 is placed at the focusing position of the vortex beam as a thick nonlinear medium. The temperature of the vapor is accurately controlled at 130 °C to ensure uniform atomic density with about 3.47×10^{14} m^{-3}. Finally, the diffraction patterns of the output vortex beam is detected by a charge-coupled device (CCD) for identifying the OAM modes in real-time.

Figure 1(b) shows the schematic diagram of OAM modes identification based on spatial self-phase modulation. The focused vortex beam passes through the atomic medium resulting in the atomic nonlinear refractive index is induced. Meanwhile, the vortex beam undergoes the nonlinear phase shift, which is directly related to the OAM mode. Thus, the diffraction rings with clearly distinguishable tails is generated for simultaneously identifying the magnitude and sign of OAM mode of the vortex beam.

Optics EXPRESS

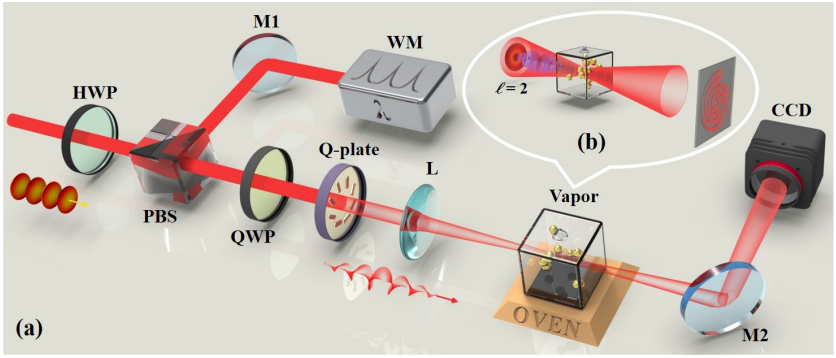

Fig. 1. (a) Sketch of experimental setup. HWP, half-wave plate; PBS, polarization beam splitter; QWP, quarter-wave plate; M, high-reflection mirror; L, lens; CCD, charge coupled device; WM, wavelength meter. (b) Schematic diagram for realizing the OAM modes identification.

3. Experimental results and discussions

The vortex beam, introducing a new degree of freedom ℓ in the light-related applications owing to the arbitrary topological charge, is expressed as [35]:

$$E_{in}(r,\varphi,z) = A_0(\frac{r}{\omega_0})^{|\ell|}exp(-\frac{r^2}{{\omega_0}^2})exp(-i\ell\varphi) \tag{1}$$

where A_0 is a constant, ω_0 is the beam waist, ℓ is the topological charge representing OAM modes. When the vortex beam transmits distance z in free space and is focused by a thin lens with the focal length of f, the electric field distribution of the vortex beam at the focus can be simulated based on the Collins integral [36]:

$$\begin{aligned} E_{focus}(r,\varphi,z) = {} & \frac{i^{\ell+1}{\omega_0}^{2|\ell|+2}kA_0}{2f}exp(-ikz)exp[-\frac{ikr^2}{2f}(1-\frac{z}{f})] \\ & \times(\frac{z}{2f}\cdot\frac{r}{\omega_0})^{|\ell|}exp(-\frac{k^2{\omega_0}^2r^2}{4f^2})L_0^{|\ell|}(\frac{k^2{\omega_0}^2r^2}{4f^2})exp(-i\ell\varphi) \end{aligned} \tag{2}$$

where $L_p^{|\ell|}$ denotes the Laguerre polynomial of order $|\ell|$ and p, and $k = 2\pi/\lambda$ is the wave vector.

When the focused vortex beam passes through a thick nonlinear medium with the thickness of L, it can be regarded as a stack of some thin medium, and the waist radius interacting with the atoms is approximated to the fixed waist radius of the focus position. Therefore, the nonlinear phase shift is written as [37]:

$$\Delta\phi(r,\varphi) = (\ell\varphi + \Delta\phi_0) \times |E_{focus}(r,\varphi,z)|^2 \tag{3}$$

where $|E_{focus}(r,\varphi,z)|^2_{max} = \frac{P}{\pi\omega_0^2}$ is the laser intensity at focus position, P is the incident laser power, the $\Delta\phi_0 = n_2kL \times |E_{focus}(r,\varphi,z)|^2{}_{max}$ is the peak nonlinear phase shift corresponding to the maximum light intensity position, and the $n_2 = 8.49 \times 10^{-16}$ cm^2/W is the nonlinear refractive index. Meanwhile, $n_2 = \frac{12\pi^4}{n_0^2c}Re\chi^{(3)}$ is determined by the third-order susceptibility $\chi^{(3)} = -\frac{4}{3}N(\rho_{bb}-\rho_{aa})^{eq}|\mu_{ba}|^4\frac{T_1T_2^2}{\hbar^3\varepsilon_0}\frac{T_2\Delta-i}{(1+\Delta^2T_2^2)^2}$ [38], where c is the light speed, $(\rho_{bb}-\rho_{aa})^{eq}$ is the population difference between the excited and the ground states in thermal equilibrium, $N = 3.47 \times 10^{14}$ m^{-3} is the atomic density, Δ is the frequency detuning, $T_1 = 26$ ns is the excited state lifetime, T_2 is the dipole dephasing time, and $\mu_{ba} = 2.53 \times 10^{-29}$ C $\cdot$ m is the electric dipole moment for the circularly polarized incident beam. Different polarized beams will excite the

Optics EXPRESS

atoms through different transition paths, leading to the different transition dipole moments and third-order nonlinear susceptibility. Clearly, the nonlinear phase shift of the atomic medium is reflected by the third-order nonlinear susceptibility $\chi^{(3)}$, which is significantly adjusted by the experimental parameters of the atomic number density, frequency detuning, and laser intensity. Note that, the topological charge ℓ, representing the OAM modes, is directly related to the nonlinear phase shift.

The complex amplitude of electric field at the exit surface of the medium will be expressed as:

$$E_{out}(r,\varphi,z) = E_{focus}(r,\varphi,z) \times exp(\Delta\phi(r,\varphi)). \tag{4}$$

The electric field distribution of output vortex beam after Fresnel–Kirchhoff diffraction is expressed as [39]:

$$\begin{aligned} E(r,\varphi,d) &= \frac{1}{i\lambda d}\int_0^{\infty}\int_0^{2\pi} E_{focus}(r,\varphi,z) \times exp(\Delta\phi(r,\varphi))exp(-ikr\theta\cos\varphi)rdrd\varphi \\ &= FFT^{-1}\{H(u,v)\cdot FFT[E_{focus}(r,\varphi,z) \times exp(\Delta\phi(r,\varphi)]\} \end{aligned} \tag{5}$$

where $H(u,v) = exp\{jkd[1-\frac{\lambda^2}{2}(u^2+v^2)]\}$ is the transfer function of Fresnel–Kirchhoff propagation, d is the distance from the medium exit plane to the far-field observation plane, θ is the far-field diffraction angle, and φ is the angular coordinate on the exit plane of the medium.

Finally, the corresponding far-field intensity distribution of vortex beams can be expressed by means of the Fresnel–Kirchhoff diffraction formula:

$$I_(r,\varphi,d) = |\frac{1}{i\lambda d}|^2|\int_0^{\infty}\int_0^{2\pi} E_{focus}(r,\varphi,z) \times exp(\Delta\phi(r,\varphi))exp(-ikr\theta\cos\varphi)rdrd\varphi|^2. \tag{6}$$

It can be found that the output diffraction intensity distribution is affected by the nonlinear phase shift $\Delta\phi(r,\varphi)$. The tail number of output diffraction intensity patterns is proportional to the number of OAM modes.

Figure 2(a) is the intensity profiles of the vortex beams with OAM modes of $|\ell| = 1, 2, 3, 4$, and 5, which are theoretically simulated by Eq. (1). The corresponding diffraction intensity patterns with OAM modes from +1 to +5 are shown in Fig. 2(b). It can be seen that the diffraction rings of the vortex beams show clearly distinguishable tails after passing through the nonlinear medium, and the number of tails is equal to the magnitude of OAM modes. When the peak nonlinear phase shift is kept constant, the nonlinear diffraction ring shrinks with the increasing ℓ because the larger nonlinear phase shift is required for detecting high-order OAM modes. Additionally, the nonlinear diffraction intensity distributions of the vortex beams with $\ell = -1$ to -5 are described by Fig. 2(c). Similar to the Fig. 2(b), the number of tails agrees with the magnitude of OAM modes but with the opposite rotation direction. It is found that vortex beams have a clockwise tail direction when the modes are positive, while the negative modes is the opposite. Thus, the magnitude and sign of OAM modes are identified by the number and rotation direction of diffraction rings tails, respectively.

The experimentally observed diffraction patterns of vortex beams with $\ell = 1, 2, 3, 4$, and 5 are shown in Fig. 3(a). The vapor temperature is fixed at 130 °C, the laser power is kept at 20 mW, and the frequency is blue detuning 0.7 GHz from ^{85}Rb $5S_{1/2}(F = 3)$ - $5P_{3/2}(F' = 4)$ hyperfine transition so as to make absorption negligible [40]. The high atomic density corresponding to high vapor temperature induces large nonlinear phase shift, thus improving the visualization degree of diffraction pattern. The impact of thermal effects on diffraction pattern is not considered because of the same thermal motion and Doppler broadening at constant temperature. The spiral rings with clearly distinguishable tails are observed in the generated diffraction patterns with clockwise rotation direction. Meanwhile, the number of the tails agrees with the magnitude of ℓ. Furthermore, the diffraction patterns of vortex beams with $\ell = -1, -2, -3, -4$, and -5 are

Optics EXPRESS

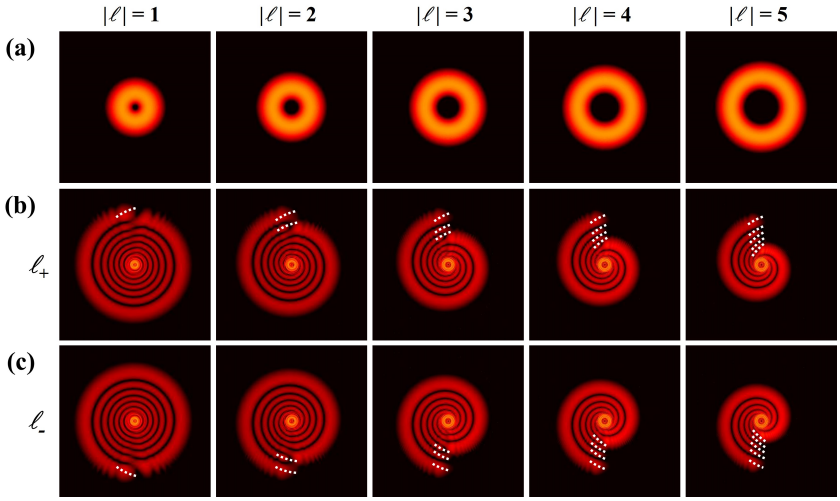

Fig. 2. (a) Theoretical simulated intensity profiles of vortex beams with $|\ell| = 1, 2, 3, 4$, and 5. The diffraction patterns of vortex beams with (b) ℓ_+ and (c) ℓ_-.

shown in Fig. 3(b). The experimental conditions are the same as in Fig. 3(a) except for the sign of ℓ. It is found that the similar spiral rings with counterclockwise rotation tails are obtained. Note that, the visualization degree of the OAM modes identification, determined by the nonlinear phase shift, is reflected by shrinkage of diffraction ring with the increasing topological charge ℓ. Obviously, the diffraction patterns of high-order OAM mode gradually becomes unclear, which can be seen from $\ell = \pm 4$ and $\ell = \pm 5$ in Fig. 3. The larger nonlinear phase shift is required to induce the diffraction ring generation as the OAM modes to be identified increasing, indicating that it is necessary to regulate nonlinear phase shift for identifying OAM modes by adjusting experimental parameters.

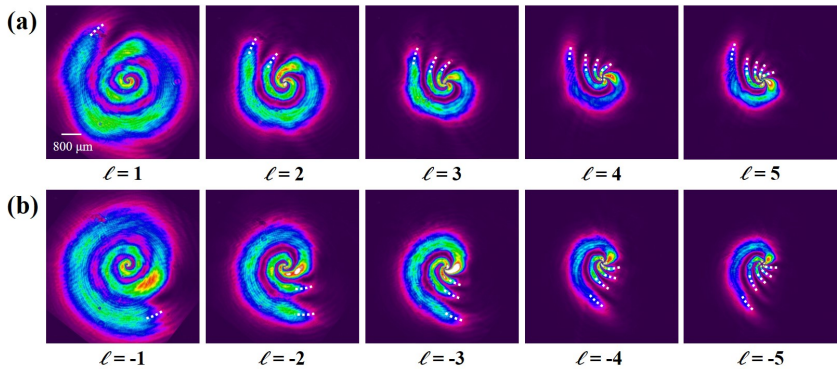

Fig. 3. Diffraction patterns of vortex beams with (a) $\ell = 1, 2, 3, 4, 5$ and (b) $\ell = -1, -2, -3, -4, -5$ when the laser power is 20 mW and the frequency is 0.7 GHz blue detuning from ^{85}Rb $5S_{1/2}(F = 3)$ - $5P_{3/2}(F' = 4)$ hyperfine transition.

The flexible tunability of atomic medium makes it possible to improve the visualization degree of OAM modes identification. Figure 4 shows the diffraction patterns of vortex beams with different laser powers. The other experimental conditions are the same as in Fig. 3. The merged tails are observed in the diffraction patterns of $\ell = +4$ with low laser power, which is shown in Fig. 4(a). The visualization degree of diffraction ring is limited at low power due to

Optics EXPRESS

enhanced absorption, which is optimized by altering frequency detuning and laser power. As the laser power further increasing, the four clearly distinguishable tails are observed in expanded diffraction patterns with gradually improved visualization degree of OAM modes identification, which attribute to the enhanced nonlinear effect [23]. Meanwhile, the cases of $\ell = +5$ vortex beam with five tails (Fig. 4(b)) demonstrate similar behaviors but with different profile. The profile area of the diffraction patterns increases with the increasing laser power. Note that, the diffraction patterns profile area of $\ell = +5$ is smaller than that of $\ell = +4$ with same laser power. It means that high laser power induced larger nonlinear phase shifts is necessary to generate diffraction rings as increasing topological charge ℓ [41].

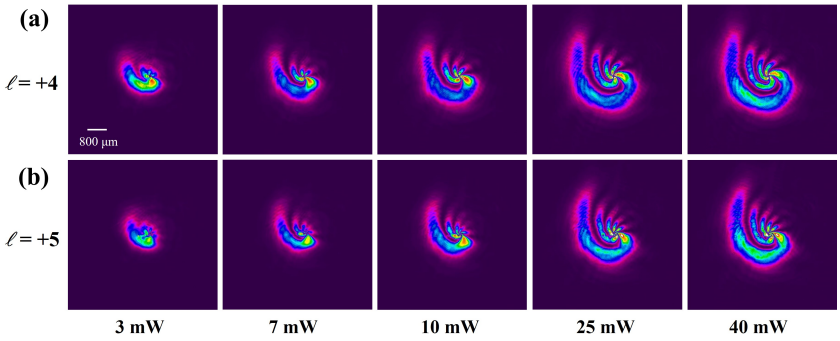

Fig. 4. The diffraction patterns of vortex beams with (a) $\ell = +4$ and (b) $\ell = +5$ when the laser power is 3, 7, 10, 25, and 40 mW, respectively.

The diffraction patterns of vortex beam are further investigated by adapting frequency detunings, which are presented in Fig. 5. The other experimental conditions are the same as in Fig. 3. When the blue detuning from ^{85}Rb $5S_{1/2}(F = 3)$ - $5P_{3/2}(F' = 4)$ hyperfine transition is decreased from 1.1 to 0.7 GHz, the profile area of diffraction patterns increases with a gradually clear tail as illustrated in Fig. 5(a). As the frequency detuning decreases, the nonlinear effect of the atomic vapor becomes significant with enhanced interaction between laser and atoms [42]. The visualization degree of the OAM modes identification is improved with the decreasing laser detuning. Meanwhile, the case of red detuning from ^{87}Rb $5S_{1/2}(F = 2)$ - $5P_{3/2}(F' = 1)$ hyperfine transition has a similar behavior, which is shown in Fig. 5(b). In addition, it can be found that the profile area of blue detuning diffraction pattern is larger than that the situation of same red detuning. The isotope ^{85}Rb atoms exhibits the stronger nonlinear effect with the 2.5 times

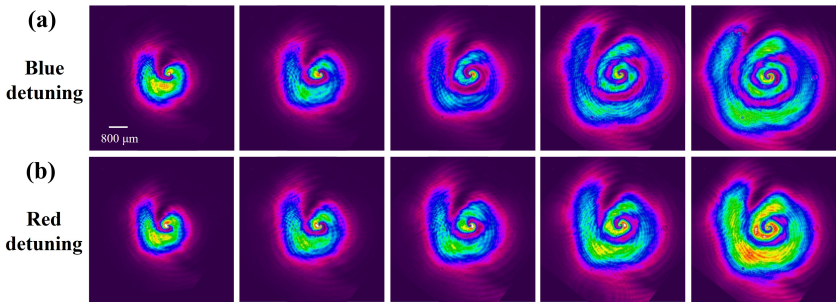

Fig. 5. The diffraction patterns of $\ell = +1$ vortex beam with (a) 1.1, 1.0, 0.9, 0.8, 0.7 GHz blue detuning from ^{85}Rb $5S_{1/2}(F = 3)$ - $5P_{3/2}(F' = 4)$ hyperfine transition and (b) −1.1, −1.0, −0.9, −0.8, −0.7 GHz red detuning from ^{87}Rb $5S_{1/2}(F = 2)$ - $5P_{3/2}(F' = 1)$ hyperfine transition.

Optics EXPRESS

abundance greater than that of ^{87}Rb in an Rb vapor [43]. To sum up, the atomic vapor with flexible and tunable nonlinear effect, achieving by varying laser power and frequency detuning, makes it an attractive candidate for identifying the OAM modes information of vortex beams. Meanwhile, we believe that higher order OAM modes identification can be realized in atomic medium with high damage thresholds compared with the use of two-dimensional material.

4. Conclusions

In summary, we experimentally demonstrate the OAM modes identification of the vortex beams in Rb vapor based on spatial self-phase modulation. The refractive index of atomic medium is spatially modulated by the focused vortex beam, resulting in the nonlinear phase shift related to the OAM modes directly when the vortex beam passes through the atomic medium. The nonlinear diffraction patterns are induced for identifying the magnitude and signs of OAM modes with the ℓ = 1, 2, 3, 4 and 5 by the number and direction of clearly distinguishable tails, respectively. Moreover, the diffraction patterns of vortex beams are dynamically manipulated by regulating the laser power or frequency detuning for further improving the visualization degree of high-order OAM modes identification. This work holds tremendous promises for identifying the high-order OAM modes of vortex beams through the nonlinear effect of atomic medium.

Funding. National Natural Science Foundation of China (62075121); Open Fund of MOE Key Laboratory of Weak-Light Nonlinear Photonics (OS 22-2); Shanxi "1331 Project".

Acknowledgments. We would like to thank the Professor Shuqing Chen and the Doctor MingYang Su from Shenzhen University for helpful discussions of theoretical simulation.

Disclosures. The authors declare no conflicts of interest.

Data availability. Data underlying the results presented in this paper are not publicly available at this time but may be obtained from the authors upon reasonable request.

References

1. R. C. Devlin, A. Ambrosio, N. A. Rubin, J. P. B. Mueller, and F. Capasso, "Arbitrary spin-to-orbital angular momentum conversion of light," Science **358**(6365), 896–901 (2017).
2. A. Chong, C. H. Wan, J. Chen, and Q. W. Zhan, "Generation of spatiotemporal optical vortices with controllable transverse orbital angular momentum," Nat. Photonics **14**(6), 350–354 (2020).
3. S. Zhang, P. C. Huo, W. Q. Zhu, C. Zhang, P. Chen, M. Z. Liu, L. Chen, H. J. Lezec, A. Agrawal, Y. Q. Lu, and T. Xu, "Broadband detection of multiple spin and orbital angular momenta via dielectric metasurface," Laser Photonics Rev. **14**(9), 2000062 (2020).
4. L. Allen, M. W. Beijersbergen, R. J. Spreeuw, and J. P. Woerdman, "Orbital angular momentum of light and the transformation of Laguerre-Gaussian laser modes," Phys. Rev. A **45**(11), 8185–8189 (1992).
5. X. Li, H. Ma, H. Zhang, M. Tang, H. Li, J. Tang, and Y. Wang, "Is it possible to enlarge the trapping range of optical tweezers via a single beam?" Appl. Phys. Lett. **114**(8), 081903 (2019).
6. Y. Shen, Z. Wan, Y. Meng, X. Fu, and M. Gong, "Polygonal vortex beams," IEEE Photonics J. **10**(4), 1–16 (2018).
7. A. Mair, A. Vaziri, G. Weihs, and A. Zeilinger, "Entanglement of the orbital angular momentum states of photons," Nature **412**(6844), 313–316 (2001).
8. A. Vaziri, J. Pan, T. Jennewein, G. Weihs, and A. Zeilinger, "Concentration of higher dimensional entanglement: qutrits of photon orbital angular momentum," Phys. Rev. Lett. **91**(22), 227902 (2003).
9. J. Wang, "Advances in communications using optical vortices," Photonics Res. **4**(5), B14 (2016).
10. J. Yuan, H. Zhang, C. Wu, L. Wang, L. Xiao, and S. Jia, "Tunable optical vortex array in a two-dimensional electromagnetically induced atomic lattice," Opt. Lett. **46**(17), 4184–4187 (2021).
11. Y. L. He, H. P. Ye, J. M. Liu, Z. Q. Xie, P. P. Wang, B. Yang, X. X. Zhou, Y. X. Gao, S. Q. Chen, Y. Li, and D. Y. Fan, "Effectively identifying the topological charge and polarization order of arbitrary singular light beams based on orthogonal polarization separating," IEEE Photonics J. **11**(6), 1–8 (2019).
12. S. M. A. Hosseini-Saber, E. A. Akhlaghi, and A. Saber, "Diffractometry-based vortex beams fractional topological charge measurement," Opt. Lett. **45**(13), 3478–3481 (2020).
13. Q. Zhao, M. Dong, Y. H. Bai, and Y. J. Yang, "Measuring high orbital angular momentum of vortex beams with an improved multipoint interferometer," Photonics Res. **8**(5), 745–749 (2020).
14. S. W. Cui, B. Xu, S. Y. Luo, H. Y. Xu, Z. P. Cai, Z. Q. Luo, J. X. Pu, and S. Chávez-Cerda, "Determining topological charge based on an improved Fizeau interferometer," Opt. Express **27**(9), 12774–12779 (2019).
15. S. Liu, J. Han, X. Cheng, X. Wang, Q. Zhang, B. He, T. Jiao, and Z. Ren, "Mechanism of all-optical spatial light modulation in graphene dispersion," J. Phys. Chem. C **125**(30), 16598–16604 (2021).

Optics EXPRESS

16. Y. Shan, L. Wu, Y. Liao, J. Tang, X. Dai, and Y. Xiang, "A promising nonlinear optical material and its applications for all-optical switching and information converters based on the spatial self-phase modulation (SSPM) effect of $TaSe_2$ nanosheets," J. Mater. Chem. C **7**(13), 3811–3816 (2019).
17. Y. Jia, Z. Li, M. Saeed, J. Tang, H. Cai, and Y. Xiang, "Kerr nonlinearity in germanium selenide nanoflakes measured by Z-scan and spatial self-phase modulation techniques and its applications in all-optical information conversion," Opt. Express **27**(15), 20857–20873 (2019).
18. Y. Liao, C. Song, Y. Xiang, and X. Dai, "Recent advances in spatial self-phase modulation with 2D materials and its applications," Ann. Phys. **532**(12), 2000322 (2020).
19. G. Wang, S. Zhang, X. Zhang, L. Zhang, Y. Cheng, D. Fox, H. Zhang, J. N. Coleman, W. J. Blau, and J. Wang, "Tunable nonlinear refractive index of two-dimensional MoS_2, WS_2, and $MoSe_2$ nanosheet dispersions," Photonics Res. **3**(2), A51 (2015).
20. L. Lu, W. Wang, L. Wu, X. Jiang, Y. Xiang, J. Li, D. Fan, and H. Zhang, "All-optical switching of two continuous waves in few layer bismuthene based on spatial cross-phase modulation," ACS Photonics **4**(11), 2852–2861 (2017).
21. Y. Liao, Q. Ma, Y. Shan, J. Liang, X. Dai, and Y. Xiang, "All-optical applications for passive photonic devices of TaS_2 nanosheets with strong Kerr nonlinearity," J. Alloys Compd. **806**, 999–1007 (2019).
22. L. Wu, X. Yuan, D. Ma, Y. Zhang, W. Huang, Y. Ge, Y. Song, Y. Xiang, J. Li, and H. Zhang, "Recent advances of spatial self-phase modulation in 2D materials and passive photonic device applications," Small **16**(35), 2002252 (2020).
23. M. Y. Su, Z. Guo, J. M. Liu, Y. L. He, X. X. Zhou, H. P. Ye, Y. Li, X. M. Zhang, S. Q. Chen, and D. Y. Fan, "Identification of optical orbital angular momentum modes with the Kerr nonlinearity of few-layer WS_2," 2D Mater. **7**(2), 025012 (2020).
24. S. Ning, J. Lu, S. Liang, Y. Feng, C. Li, Z. Zhang, and Y. Zhang, "Talbot effect of an electromagnetically induced square photonic lattice assisted by a spatial light modulator," Opt. Lett. **46**(19), 5035–5038 (2021).
25. H. Hu, D. Luo, C. Pan, Y. Qin, Y. Zhang, D. Wei, H. Chen, H. Gao, and F. Li, "Collapse of hybrid vector beam in Rb atomic vapor," Opt. Lett. **46**(11), 2614–2617 (2021).
26. Z. Zhang, S. Liang, F. Li, S. Ning, Y. Li, G. Malpuech, Y. Zhang, M. Xiao, and D. Solnyshkov, "Spin–orbit coupling in photonic graphene," Optica **7**(5), 455–462 (2020).
27. H. Cai, J. Liu, J. Wu, Y. He, S.-Y. Zhu, J.-X. Zhang, and D.-W. Wang, "Experimental observation of momentum-space chiral edge currents in room-temperature atoms," Phys. Rev. Lett. **122**(2), 023601 (2019).
28. Z. Zhang, R. Wang, Y. Zhang, Y. V. Kartashov, F. Li, H. Zhong, H. Guan, K. Gao, F. Li, Y. Zhang, and M. Xiao, "Observation of edge solitons in photonic graphene," Nat. Commun. **11**(1), 1902 (2020).
29. S. Wang, J. Yuan, L. Wang, L. Xiao, and S. Jia, "Measurement of the Kerr nonlinear refractive index of the Rb vapor based on an optical frequency comb using the z-scan method," Opt. Express **28**(25), 38334–38342 (2020).
30. C. P. Jisha, A. Alberucci, J. Beeckman, and S. Nolte, "Self-trapping of light using the pancharatnam-berry phase," Phys. Rev. X **9**(2), 021051 (2019).
31. J. Wu, M. Guo, H. Zhou, J. Liu, J. Li, and J. Zhang, "Experimental realization of efficient nondegenerate four-wave mixing in cesium atoms," Opt. Express **30**(8), 12576–12585 (2022).
32. J. Yuan, C. Wu, L. Wang, G. Chen, and S. Jia, "Observation of diffraction pattern in two-dimensional optically induced atomic lattice," Opt. Lett. **44**(17), 4123–4126 (2019).
33. L. Zeng, M. X. Dong, Y. H. Ye, Y. C. Yu, E. Z. Li, W. H. Zhang, K. Zhang, D. S. Ding, and B. S. Shi, "Modulation of the optical beam with orbital angular momentum in hot atomic rubidium vapor," AIP Adv. **10**(1), 015135 (2020).
34. L. Marrucci, C. Manzo, and D. Paparo, "Optical spin-to-orbital angular momentum conversion in inhomogeneous anisotropic media," Phys. Rev. Lett. **96**(16), 163905 (2006).
35. L. Allen, M. Babiker, W. K. Lai, and V. E. Lembessis, "Atom dynamics in multiple Laguerre-Gaussian beams," Phys. Rev. A **54**(5), 4259–4270 (1996).
36. S. A. Collins, "Lens-system diffraction integral written in terms of matrix optics," J. Opt. Soc. Am. **60**(9), 1168–1177 (1970).
37. E. V. G. Ramirez, M. L. A. Carrasco, M. M. M. Otero, S. C. Cerda, and M. D. I. Castillo, "Far field intensity distributions due to spatial self phase modulation of a Gaussian beam by a thin nonlocal nonlinear media," Opt. Express **18**(21), 22067–22079 (2010).
38. Y. Zhang, X. Cheng, X. Yin, J. Bai, P. Zhao, and Z. Ren, "Research of far-field diffraction intensity pattern in hot atomic Rb sample," Opt. Express **23**(5), 5468–5476 (2015).
39. J. Yuan, X. Wang, L. Wang, L. Xiao, and S. Jia, "Tunable high-order Bessel-like beam generation based on cross-phase modulation," Opt. Express **30**(10), 15978–15985 (2022).
40. C. F. McCormick, D. R. Solli, R. Y. Chiao, and J. M. Hickmann, "Nonlinear absorption and refraction in near-detuned rubidium vapor," J. Opt. Soc. Am. B **20**(12), 2480–2483 (2003).
41. H. Wang, D. Goorskey, and M. Xiao, "Enhanced Kerr nonlinearity via atomic coherence in a three-level atomic system," Phys. Rev. Lett. **87**(7), 073601 (2001).
42. X. Cheng, Q. Zhang, H. Chen, B. He, Z. Ren, Y. Zhang, and J. Bai, "Demonstration of Bessel-like beam with variable parameters generated using cross-phase modulation," Opt. Express **25**(21), 25257–25266 (2017).
43. C. F. McCormick, D. R. Solli, R. Y. Chiao, and J. M. Hickmann, "Saturable nonlinear refraction in hot atomic vapor," Phys. Rev. A **69**(2), 023804 (2004).